Environmental Science & Technology

pubs.acs.org/est

Article

Structural Effects of Amines in Enhancing Methanesulfonic Acid-Driven New Particle Formation

Jiewen Shen, Jonas Elm, Hong-Bin Xie,* Jingwen Chen, Junfeng Niu, and Hanna Vehkamäki

Cite This: *Environ. Sci. Technol.* 2020, 54, 13498−13508

Read Online

ACCESS | Metrics & More | Article Recommendations | Supporting Information

ABSTRACT: Atmospheric amines can enhance methanesulfonic acid (MSA)-driven new particle formation (NPF), but the mechanism is fundamentally different compared to that of the extensively studied sulfuric acid (SA)-driven process. Generally, the enhancing potentials of amines in SA-driven NPF follow the basicity, while this is not the case for MSA-driven NPF, where structural effects dominate, making MSA-driven NPF more prominent for methylamine (MA) compared to dimethylamine (DMA). Therefore, probing structural factors determining the enhancing potentials of amines on MSA-driven NPF is key to fully understanding the contribution of MSA to NPF. Here, we performed a comparative study on DMA and MA enhancing MSA-driven NPF by examining cluster formation using computational methods. The results indicate that DMA−MSA clusters are more stable than the corresponding MA−MSA clusters for cluster sizes up to $(DMA)_2(MSA)_2$, indicating that the basicity of amines dominates the initial cluster formation. The methyl groups of DMA were found to present significant steric hindrance beyond the $(DMA)_2(MSA)_2$ cluster and this adds to the lower hydrogen bonding capacity of DMA, making the cluster growth less favorable compared to MA. This study implies that several amines could synergistically enhance MSA-driven NPF by maximizing the advantage of different amines in different amine−MSA cluster growth stages.

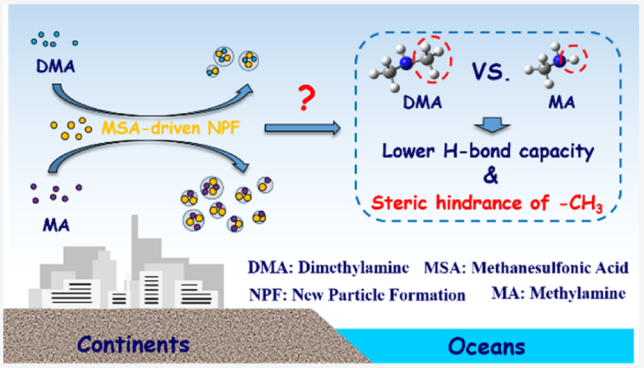

INTRODUCTION

Aerosols have significant effects on the global climate, visibility, and human health.[1−6] Atmospheric new particle formation (NPF) through gas-to-particle conversion constitutes over half of the global aerosol budget.[1−12] It is widely accepted that gaseous sulfuric acid (SA) formed from SO_2 oxidation plays a key role in atmospheric NPF,[3,5,6,13−22] and a broad variety of atmospheric compounds such as ammonia, amines, and organic acids efficiently enhance SA-driven NPF by stabilizing the newly formed molecular clusters.[3,13,14,20,23−28] However, significant gaps remain between the observed particle formation rates in the field and laboratories and the rates predicted by simulations.[6,11,19,28−32] Therefore, there is a need to consider the involvement of other gaseous precursors in NPF to reduce the gaps between experiments and simulations.

Methanesulfonic acid (MSA) has been identified to be another potentially important precursor driving NPF in both coastal and continental atmospheres.[29,31,33−36] With the implementation of stricter regulations on anthropogenic SO_2 emissions, the contribution of MSA to NPF will be higher in the future.[29,35,37] The oxidation of organosulfur compounds (OSCs), mainly emitted from marine organisms, forest vegetation, agricultural and domestic activities, and even human breath, is the main source of MSA.[31,35,38−40] The gaseous MSA concentration typically ranges from 10 to 100% of that of SA (the latter is about 10^5 to 10^7 cm^{-3} in the atmosphere).[29,31,41] Because the two-component MSA−H_2O system does not form particles efficiently under typical atmospheric conditions,[31] the contribution of MSA to NPF has been found to highly depend on the participation of other vapors to enhance NPF.[29,31,41−43] Therefore, to fully understand the contribution of MSA to NPF, it is crucial to reveal structure-enhancing potential relationship of atmospheric vapors and further identify novel atmospheric species with strong enhancing potential on MSA-driven NPF.[29,43]

Although SA-driven NPF has been extensively studied,[2,3,5,13,14,23,44−47] research on chemical species that can efficiently enhance MSA-driven NPF has been relatively limited. The Finlayson-Pitts group and Benny Gerber group have however performed several experimental and simulation studies, respectively, to assess the enhancing potentials of common atmospheric bases such as ammonia, methylamine

Received: August 9, 2020
Revised: October 8, 2020
Accepted: October 9, 2020
Published: October 22, 2020

(MA), dimethylamine (DMA), and trimethylamine (TMA).[10,31,34,42,43,48−54] MA was found to be the strongest enhancing species on MSA-driven NPF,[10,43] in contrast to DMA being the most effective enhancer for SA-driven NPF.[14,27] Our recent computational study suggests that the enhancing potential of monoethanolamine (MEA) should be even higher than that of MA.[29] Thus, it has been established that the enhancing potential of investigated atmospheric bases does not simply follow the order of their gas-phase basicity [gas-phase basicity (GB) for DMA is 896.5 kJ mol^{-1} and for MA is 864.5 kJ mol^{-1} and for MEA is 896.8 kJ mol^{-1}], although acid−base reactions occur between atmospheric bases and MSA in NPF.[29,43,55] This implies that the enhancing potential of bases in MSA-driven NPF is highly dependent on the exact molecular structure of the amine.

The only structural difference between DMA and MA is the additional methyl ($-CH_3$) group in DMA compared to an H atom in MA. Finlayson-Pitts et al. proposed that the lower hydrogen bond (H-bond) capacity is the main reason that DMA (one −NH bond site) has a lower enhancing potential than MA (two −NH bond sites).[43] Recently, we confirmed that the H-bond capacity plays an important role in determining the enhancing potentials of amines on MSA-driven NPF.[29] In fact, the change from an H atom to a $-CH_3$ group leads to not only lower H-bond capacity but also higher steric hindrance in DMA compared to MA.[56,57] Because MSA also contains an additional $-CH_3$ group compared to SA, the role of steric hindrance of $-CH_3$ groups of DMA should be more pronounced when DMA interacts with MSA, especially in clusters with several DMA and MSA molecules.[56,57] However, to the best of our knowledge, no previous study has addressed how steric hindrance interplays with H-bond capacity and basicity in determining the enhancing potentials of amines on MSA-driven NPF.

In this study, we performed a comparative study on DMA and MA enhancing MSA-driven NPF to probe the role of $-CH_3$ groups of DMA in the enhancing potential of gaseous species by examining the formation of DMA−MSA and MA−MSA clusters. We have obtained the global minimum structures of $(DMA)_m(MSA)_n$ (m = 1−4, n = 1−4) clusters. The corresponding thermodynamics data, together with previously reported results for pure $(MSA)_{1-4}$, $(DMA)_{1-4}$ clusters and $(MA)_{1-4}(MSA)_{0-4}$ clusters (lower energy structures for some cases are obtained in this work),[29,44,58] were used as inputs to the atmospheric cluster dynamic code (ACDC) to obtain the cluster distribution dynamics and growth pathways for both the DMA−MSA and MA−MSA systems.[59]

COMPUTATIONAL DETAILS

Configurational Sampling. The pure $(MSA)_{1-4}$, $(DMA)_{1-4}$, and $(MA)_{1-4}$ clusters are from previous studies.[29,44,58] Here, a multistep global minimum sampling scheme was employed to determine the global minima of $(DMA)_m(MSA)_n$ (m = 1−4, n = 1−4) clusters. This approach has been applied in our previous studies addressing atmospheric cluster formation.[13,23,29] The scheme can be described as a gradual screening process using a series of theoretical methods. Around 10,000 initial configurations were randomly generated for each cluster, and subsequently, the geometries were optimized at the semiempirical PM6 level of theory. Based on single-point energy calculations at the ωB97X-D/6-31+G(d) level of theory calculated for the geometries obtained at the PM6 level of theory, the lowest 100 conformers were selected for full geometry optimization and vibrational frequency calculations at the ωB97X-D/6-31++G(d,p) level of theory. Single-point energy calculations at the DLPNO-CCSD(T)/aug-cc-pVTZ level of theory were further performed on selected low-free energy conformations at the ωB97X-D/6-31++G(d,p) level of theory. Finally, the conformation with the lowest Gibbs free energy (combining single-point energy at the DLPNO-CCSD(T)/aug-cc-pVTZ level with Gibbs free energy correction at the ωB97X-D/6-31++G(d,p) level of theory) was selected as the global minimum for a given cluster. All calculations employing the semiempirical PM6 and density functional theory (ωB97X-D functional) methods were performed with the GAUSSIAN 09 program package,[60] and the DLPNO-CCSD(T)/aug-cc-pVTZ single-point energy calculations were performed with the ORCA 4.0.0 program with tight PNO and SCF convergence criteria.[61] The DLPNO-CCSD(T)/aug-cc-pVTZ//ωB97X-D/6-31++G(d,p) level of theory was chosen as it has been shown to yield accurate thermochemistry for atmospheric molecular clusters compared to higher level methods.[62] In addition, we also conducted a global minimum search for the previously studied MA−MSA system using the same scheme as that for the DMA−MSA cluster system. For all $(MA)_{1-4}(MSA)_{1-4}$ clusters except for the $(MA)_1(MSA)_1$ and $(MA)_4(MSA)_4$ clusters, lower-energy conformations were identified compared to those published by Chen et al.,[43] and the lowest free energy structures found were used in this study. The formation free energy (ΔG) for each cluster was obtained by subtracting the Gibbs free energy of the constituent monomers from that of the cluster at 298.15 K, and the ΔG values at other temperatures were also calculated, assuming that the enthalpy and entropy change (ΔH and ΔS) stays constant under the studied temperature range (258.15−298.15 K).

ACDC Simulations. The ACDC was employed to study the cluster formation rates, steady-state cluster concentrations, and cluster growth pathways.[59] The detailed description of the ACDC program is presented in a previous study.[59] The employed basic formula of the ACDC is presented in the Supporting Information. Here, the simulated system for clusters is $(DMA)_m(MSA)_n$ (m = 0−4, n = 0−4), that is, the maximal number of base (DMA) and acid (MSA) molecules in the clusters is set to 4. The $(DMA)_4(MSA)_5$ and $(DMA)_5(MSA)_5$ were defined to be stable enough to contribute to the cluster formation rate (see detailed discussion on the judgement of the cluster stability and selection of boundary clusters in the Supporting Information). The concentration of DMA and MSA monomers was set to be 1 ppt (~2.50×10^7 cm^{-3}), 10 ppt (~2.50×10^8 cm^{-3}), and 100 ppt (~2.50×10^9 cm^{-3}) and 10^5, 10^6, 10^7, and 10^8 cm^{-3}, respectively. The simulations were mainly performed at 278.15 K, with additional runs at 258.15, 268.15, 288.15, and 298.15 K, to investigate the effect of temperature. Because the value of the coagulation sink coefficient (C_{coag}) for MSA vapor is not reported, a constant C_{coag} of 2.60×10^{-3} s^{-1}, corresponding to a typical value observed in the boreal forest, was chosen as a sink term in the ACDC simulations.[29,59] Moreover, the effect of C_{coag} on results was also examined, by additional runs with various values covering cases of clean and haze days (6×10^{-4} to 6×10^{-2} s^{-1}).[63,64] For the $(MA)_x(MSA)_y$ (x = 0−4, y = 0−4) clusters, the $(MA)_4(MSA)_5$ and $(MA)_5(MSA)_5$ clusters were set as boundary clusters, with the remaining settings also identical to the DMA−MSA system. To investigate the effect

https://dx.doi.org/10.1021/acs.est.0c05358
Environ. Sci. Technol. 2020, 54, 13498−13508

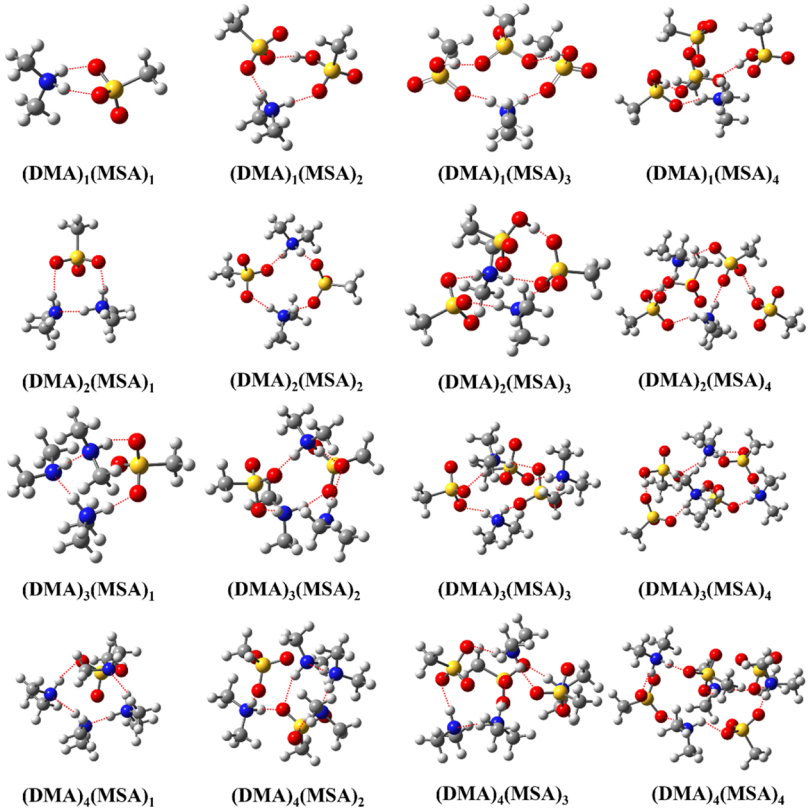

Figure 1. Lowest Gibbs free energy conformations of the $(DMA)_m(MSA)_n$ (m = 1−4, n = 1−4) clusters at the DLPNO-CCSD(T)/aug-cc-pVTZ//ωB97X-D/6-31++G(d,p) level of theory. The red balls represent oxygen atoms, blue ones are for nitrogen atoms, gray ones are for carbon atoms, and white ones are for hydrogen atoms. Dashed red lines indicate H-bonds (defined by the configurational criteria).

of the studied cluster size on the difference in cluster formation rate and steady-state cluster concentrations between the DMA−MSA and MA−MSA systems, ACDC simulations were also performed for systems with the maximal number of acid and base molecules in the cluster set to 2 and 3. Evaporation rates of clusters, as the fundamental data for understanding the results of ACDC simulations, are presented in the Supporting Information (Figure S5) with their corresponding evaporation pathways (Table S1).

Analysis of the Steric Hindrance Effect. For isolated molecules, steric hindrance can be estimated in the form of the deformation energy. The deformation energy can be calculated as the difference in energy between that of the global minimum structure and the deformed conformer.[65,66] However, as the clusters are held together primarily via H-bonds and electrostatic interactions, no analogical method exists to directly calculate the deformation energy in molecular clusters. In fact, the cluster geometry was determined as a result of making a compromise between the steric hindrance and attractive interaction such as H-bonds and electrostatic forces. In this view, repulsive interaction energy (E_{rep}) should be greater, average intermolecular C−C distance (D_{C-C}) between $-CH_3$ and $-CH_3$ should be shorter, and average H-bond length (L_H) should be longer for the system with the steric hindrance than those for a similar system without the steric hindrance, respectively. Therefore, here, three parameters including E_{rep}, D_{C-C}, and L_H were employed to indirectly probe the effect of steric hindrance. E_{rep} was calculated using energy decomposition analysis based on a classical force field (EDA-FF) using Multiwfn software (see computational details in the Supporting Information).[67−71] The average C−C distance was calculated for all intermolecular carbon atoms in a given cluster. For the average L_H calculation, the H-bond is defined by the following configurational criteria: distance between the two heavy atoms X and Y is below 3.5 Å (X, Y = N or O and X ≠ Y), the X−Y−H or Y−X−H angle is smaller than 30°, and the distance for X−H···Y or Y−H···X is shorter than 2.45 Å.[72] In addition, intermolecular N−N distance (D_{N-N}), S−S distance (D_{S-S}), O−O distance (D_{O-O}), and the cluster density (ρ) were calculated to check the effect of steric hindrance on the intermolecular spacing of clusters (Figure S7). Multiwfn software was employed to calculate ρ values based on the theory mentioned in the refs 67, 73.

RESULTS AND DISCUSSION

Cluster Structures. The obtained global minima of $(DMA)_m(MSA)_n$ (m = 1−4, n = 1−4) clusters and $(MA)_x(MSA)_y$ (x = 1−4, y = 1−4) clusters [$(MA)_1(MSA)_1$ and $(MA)_4(MSA)_4$ cluster structures are from Chen et al.'s work] are presented in Figures 1 and S8, respectively. Because the pure $(DMA)_{1-4}$, $(MA)_{1-4}$, and $(MSA)_{1-4}$ clusters have been discussed in previous studies,[29,44,58] we mainly focus on the heteromolecular $(base)_{1-4}(MSA)_{1-4}$ (base = DMA/MA) clusters. Generally, the base−acid clusters are stabilized by both intermolecular H-bonds and electrostatic interactions between positive and negative ions formed by proton transfer reactions from MSA to bases. For all heteromolecular $(DMA)_{1-4}(MSA)_{1-4}$ clusters, proton transfers are observed. When $N_{DMA} \geq N_{MSA}$ (N_{DMA} and N_{MSA} represent the number of DMA and MSA monomers in a cluster, respectively), all protons in MSA molecules are transferred to DMA molecules, and ($N_{DMA}-N_{MSA}$) DMA molecules remain unprotonated.

https://dx.doi.org/10.1021/acs.est.0c05358
Environ. Sci. Technol. 2020, 54, 13498−13508

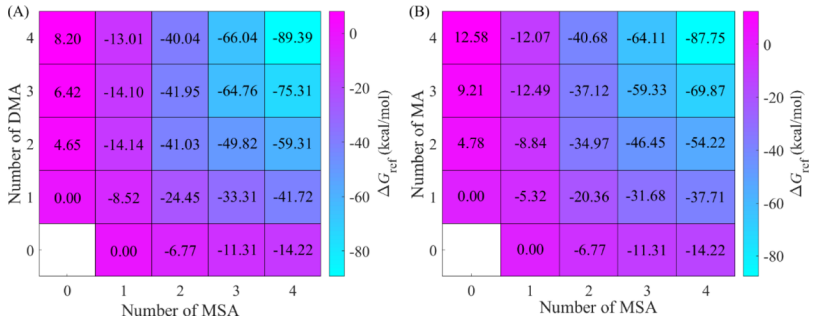

Figure 2. Formation free energy (ΔG) (kcal mol^{-1}) of the $(DMA)_{0-4}(MSA)_{0-4}$ clusters (A) and $(MA)_{0-4}(MSA)_{0-4}$ clusters (B) calculated at the DLPNO-CCSD(T)/aug-cc-pVTZ//ωB97X-D/6-31++G(d,p) level of theory. The calculations are performed at 298.15 K and 1 atm.

When $N_{DMA} < N_{MSA}$, all DMA molecules are protonated and $(N_{MSA}-N_{DMA})$ MSA molecules are intact. Therefore, the number of proton transfers in a heteromolecular DMA−MSA cluster is equal to the lowest number of N_{DMA} and N_{MSA} and is equal to either N_{DMA} or N_{MSA} in cases where there are equal numbers of bases and acids in the cluster ($N_{DMA} = N_{MSA}$). The proton transfer pattern for the DMA−MSA clusters is similar to that of the MEA−MSA clusters in our previous study.[29] The proton transfer pattern for the MA−MSA system is almost the same as that for the DMA−MSA system except for the $(MA)_1(MSA)_1$ cluster, where proton transfer did not occur. This can be attributed to the lower basicity of MA, compared to DMA. The formation free energy difference of the $(MA)_1(MSA)_1$ cluster with and without proton transfer was discussed in our previous study.[29]

Another common structural feature observed in all heteromolecular $(base)_{1-4}(MSA)_{1-4}$ clusters in both systems is that all protonated or unprotonated amino groups (−NH and $-NH_2^+$ for DMA and $-NH_2$ and $-NH_3^+$ for MA) of bases at least participate in one H-bond formation as H-bond donors. In some cases [the $(DMA)_{2-4}(MSA)_1$ and $(DMA)_4(MSA)_{2-3}$ clusters and the $(MA)_{2-4}(MSA)_1$, $(MA)_3(MSA)_2$, and $(MA)_4(MSA)_{2-3}$ clusters], the unprotonated amino groups can act as H-bond acceptors to form extended H-bonded networks with protonated amino groups. However, within the studied maximum cluster size of four acids and four bases, the number of H-bonds (Table S2) in the DMA-containing clusters is less than that in the corresponding MA-containing clusters except for the $(DMA)_{1-2}(MSA)_{1-2}$ clusters. This is caused by the fewer available H-bond sites in DMA compared to MA. With increasing cluster size, the discrepancy in the number of formed H-bonds in the DMA−MSA clusters and the corresponding MA-MSA clusters becomes more pronounced. This is consistent with recently reported lower H-bond capacity of DMA compared to that of MA.[43] Such a difference in the number of formed H-bonds was also found in the DMA−SA and MA-SA systems (Table S2).[44] In addition, DMA−MSA clusters tend to form a spindle-like structure with increasing cluster size, in contrast to the spherical three-dimensional structure for MA−MSA clusters. The formation of a spindle-like structure results from both having less H-bond sites available and the steric hindrance caused by the additional $-CH_3$ group in DMA, compared to MA.

Cluster Formation Free Energy Surface. The formation free energy surface at 298.15 K for the DMA−MSA system is shown in Figure 2A, along with that for the MA−MSA cluster system as a comparison (Figure 2B). The corresponding ΔH and ΔS values are presented in Table S3. Figure 2 shows that most heteromolecular DMA−MSA clusters have lower ΔG than the corresponding MA−MSA clusters, within a difference in the range of 0.94−6.06 kcal mol^{-1}. However, the ΔG value for the $(DMA)_4(MSA)_2$ cluster is higher than that of the corresponding $(MA)_4(MSA)_2$ cluster. As the smallest $(DMA)_1(MSA)_1$ and $(MA)_1(MSA)_1$ clusters have a negligibly small structural effect from bases (as discussed in the Steric Hindrance Effect section), the ΔG difference between $(DMA)_1(MSA)_1$ and $(MA)_1(MSA)_1$ mainly results from the difference in gas-phase basicity of the DMA and MA compounds. The difference in ΔG values ($\Delta\Delta G_{(DMA-MSA)-(MA-MSA)}$) between DMA−MSA clusters and the corresponding MA−MSA clusters would increase (meaning more negative) significantly with increasing cluster size, if no additional structural factor plays a role. As expected, we find that the $\Delta\Delta G_{(DMA-MSA)-(MA-MSA)}$ value increases significantly from cluster size 1:1 to 2:2 along the growth pathway (see the Formation Pathways section) of the DMA−MSA clusters. However, above the 2:2 cluster size, $\Delta\Delta G_{(DMA-MSA)-(MA-MSA)}$ starts to decrease. Such a change in $\Delta\Delta G_{(DMA-MSA)-(MA-MSA)}$ with cluster size along the growth pathway leads to a similar cluster stability change of the DMA−MSA system, compared to the MA−MSA system. As indicated by evaporation rates shown in Figure S5, the DMA−MSA cluster is much stable than the corresponding MA−MSA cluster within the 2:2 cluster size; however, the trend is reversed for most clusters above the 2:2 cluster size. These imply that the specific molecular structure of the amines becomes important as the cluster formation potential does not simply follow the basicity of the base with increasing cluster size.

Steric Hindrance Effect. As discussed above, the limited number of H-bond sites in the DMA molecule is an unfavorable structural factor for the cluster formation free energy of the DMA−MSA system compared to the MA−MSA system. Beyond this, steric hindrance of the additional $-CH_3$ groups in the DMA−MSA clusters counteracts the strong enhancing potential originating from the high basicity of DMA. To look further into the effect of steric hindrance, the diagonal $(DMA)_z(MSA)_z$ and $(MA)_z(MSA)_z$ (z = 1−4) clusters were selected for further analysis, as they are essential clusters in the growth pathways for both the DMA−MSA and MA−MSA cluster systems.

As can be seen in Figure 3, the E_{rep} increases with the cluster size for both the DMA−MSA and MA−MSA systems. In all cases, except the $(base)_2(MSA)_2$ cluster, the E_{rep}-DMA is higher than E_{rep}-MA and the difference increases for the larger

https://dx.doi.org/10.1021/acs.est.0c05358
Environ. Sci. Technol. 2020, 54, 13498−13508

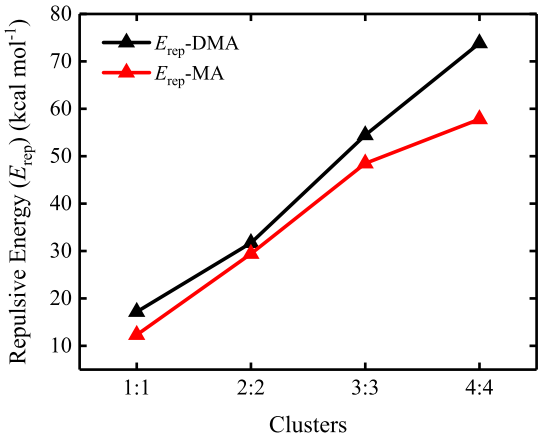

Figure 3. Repulsive energy (E_{rep}) (kcal mol^{-1}) obtained from EDA-FF analysis for the $(DMA)_z(MSA)_z$ and $(MA)_z(MSA)_z$ clusters (z = 1−4).

3:3 and 4:4 clusters. Because the only structural difference in DMA and MA is the position of an additional $-CH_3$ group in DMA compared to an H atom in MA and that the number of $-CH_3$ groups increases with the cluster size, the increased difference between E_{rep}-DMA and E_{rep}-MA with the cluster size originates from the steric hindrance effect of the additional bulky $-CH_3$ groups. This indicates that the steric hindrance effect of $-CH_3$ groups presents another unfavorable factor for the cluster formation free energy of the DMA−MSA system, compared to the MA−MSA system. For the $(DMA)_2(MSA)_2$ cluster, the H atom of the $-CH_3$ group of DMA forms an intermolecular interaction with one O atom of MSA with a distance of H···O of about 2.4 Å and the $-CH_3$ group has enough space to avoid the repulsive interaction of the $-CH_3$ groups in DMA with other groups, as shown in Figure 1, decreasing the steric hindrance in the $(DMA)_2(MSA)_2$ cluster.

Figure 4A presents the D_{C-C} for the selected clusters. With increasing cluster size, D_{C-C} increases in both systems. D_{C-C}-DMA is shorter than the corresponding D_{C-C}-MA except the $(base)_1(MSA)_1$ cluster. Notably, the difference in D_{C-C} becomes larger at larger sizes between DMA−MSA and MA−MSA systems. This is another indication that steric hindrance is more prominent in the DMA−MSA system as the bulky $-CH_3$ groups have to be closer to each other while still attempting to form strong H-bonds.

The change in the L_H with cluster size for the DMA−MSA system is presented in Figure 4B, along with one for the MA−MSA system as a comparison. In the view of cluster structures (Figure 1), for the small cluster of size 1:1 and 2:2 for the DMA−MSA system, the steric hindrance effect of $-CH_3$ groups of DMA can effectively be avoided because $-CH_3$ groups have enough space to point to various directions. However, with an increase in the cluster size such as 3:3 and 4:4, the clusters become very crowded, and the $-CH_3$ groups have to approach their neighbor molecule to make NH or NH_2^+ form H-bonds with MSA. Therefore, the L_H of the small cluster at sizes 1:1 and 2:2 for the DMA−MSA system can be considered as the reference for evaluating the steric hindrance of $-CH_3$ groups for large clusters. As can be seen from Figure 4B, the L_H-DMA of the large cluster at sizes 3:3 and 4:4 is much longer than that of reference clusters, indicating the steric hindrance effect of $-CH_3$ groups of DMA in forming large clusters.

The comparison in the L_H between DMA−MSA and MA−MSA systems further presents the steric hindrance effect of $-CH_3$ groups of DMA. For the MA−MSA system, except the $(MA)_1(MSA)_1$ cluster, the L_H-MA almost does not vary with the cluster size. For the $(MA)_1(MSA)_1$ cluster, proton transfer does not occur, making its H-bond type different from that of proton-transferred cases. This is one reason why the average H-bond length of $(MA)_1(MSA)_1$ is much shorter than that in other considered clusters. In addition, three −NHs of each protonated MA interact with O atoms of MSA in $(MA)_2(MSA)_2$, $(MA)_3(MSA)_3$, and $(MA)_4(MSA)_4$ clusters (Figure S8), even though some NH···O interactions do not form H-bonds as defined by the configurational criteria, as mentioned in the Computational Details section. This is totally different from the DMA−MSA case, where only two -NHs of each protonated DMA interact with MSA. Actually, the existence of three NH···O interactions in MA-MSA clusters should elongate the L_H-MA, compared to only two-NH···O interaction cases because the protonated MA has to adjust its orientations to make more -NHs to interact with O atoms of MSA. Even though the existence of three NH···O interactions in the MA−MSA cluster elongates the L_H-MA, the L_H-MA is still shorter than the L_H-DMA at cluster sizes of 3:3 and 4:4, further proving the steric hindrance effect of $-CH_3$ groups of DMA on forming large clusters. The analysis for all considered three parameters including E_{rep}, D_{C-C}, and L_H suggests that the steric hindrance of the $-CH_3$ groups is another unfavorable structural factor besides the available number of H-bond sites, which hinders the cluster growth in the DMA−MSA system compared to the MA−MSA system. In addition, it was found that the ρ value for all considered DMA−MSA clusters is smaller than that of the corresponding MA−MSA cluster (Figure S7). However, the difference in the ρ value between the DMA−MSA cluster and the corresponding MA−MSA

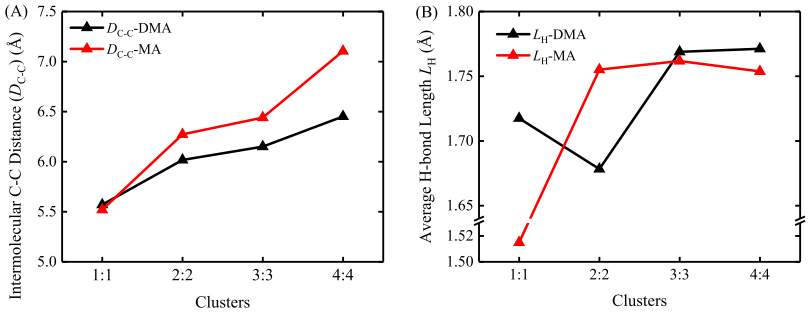

Figure 4. Variation in average intermolecular carbon−carbon distance (D_{C-C}) between $-CH_3$ and $-CH_3$ (Å) (A) and average H-bond lengths (L_H) (Å) (B) with cluster size for the $(DMA)_z(MSA)_z$ and $(MA)_z(MSA)_z$ clusters (z = 1−4).

https://dx.doi.org/10.1021/acs.est.0c05358
Environ. Sci. Technol. 2020, 54, 13498−13508

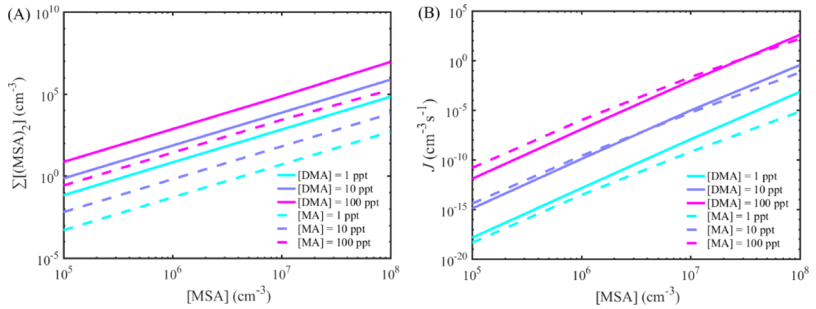

Figure 5. Simulated steady-state MSA dimer concentration ($\Sigma[(MSA)_2]$) (cm^{-3}) (A) and cluster formation rate (J) (cm^{-3} s^{-1}) (B) as a function of monomer concentrations at 278.15 K.

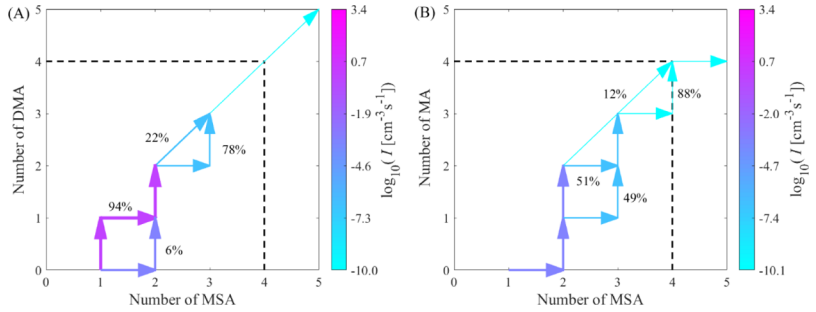

Figure 6. Cluster formation pathways for the DMA−MSA system (A) and the MA−MSA system (B) at 278.15 K, [MSA] = 10^6 cm^{-3}, and [DMA/MA] = 10 ppt. For clarity, pathways contributing less than 5% to the flux of the cluster are not shown.

cluster does not present a regular change with cluster size as that in D_{C-C}. Such an irregularity is consistent with the comprehensively irregular variation in the difference in the atom−atom distance (including D_{N-N}, D_{S-S}, and D_{O-O}, Figure S7) between two systems with cluster size. This implies that the steric repulsion could primarily affect the orientation of the $-CH_3$ groups and not the overall intermolecular spacing.

Steady-State Cluster Concentrations and Cluster Formation Rates. The steady-state concentration of all clusters including the MSA dimer ($\sum[(MSA)_2]$) and cluster formation rates (J) can be used to evaluate the enhancing potential of a given amine in MSA-driven NPF.[13,14,23−25] Figure 5 presents both $\sum[(MSA)_2]$ and J as a function of the concentration of the MSA (10^5 to 10^8 cm^{-3}) and base (DMA/MA, 1−100 ppt), simulated for clusters containing up to four acid and four base molecules for both systems. $\sum[(MSA)_2]$ of the DMA−MSA system is significantly higher than that of the MA−MSA system in all considered MSA and base concentration ranges. However, J in the DMA−MSA system is very close to that in the MA−MSA system and is found to even be lower than that of the MA−MSA system at lower MSA concentrations (below 10^7 cm^{-3}) and higher base concentrations (10 and 100 ppt). In addition, the selection of C_{coag} almost has no effect on the trend for $\sum[(MSA)_2]$ and J of the DMA−MSA system compared to MA−MSA (Supporting Information). It should be noted that J values for both systems are negligibly small under all considered conditions except the highest MSA and amine concentration. It has been shown earlier that as indicators of the enhancing potential, the concentration of all clusters that include the acid dimer ($\sum[(acid)_2]$, acid = SA/MSA) and J yield a consistent trend for a given amine.[13,14,23,29] However, this is not the case for DMA when MA is selected as a reference for evaluating its enhancing potential. The different trends mainly result from that $\sum[(MSA)_2]$ at higher concentrations cannot efficiently facilitate the growth to larger cluster in the DMA−MSA system because of the unfavorable ΔG of the larger cluster as discussed in the Cluster Formation Free Energy Surface section. This is supported by the findings that the difference in $\sum[(MSA)_2]$ only varies slightly and that J is significantly decreased (or even reversed) between the MA−MSA and DMA−MSA systems, when increasing the largest simulated cluster size from 2:2 to 4:4 (Figures S9, S10 and 5). The trend of decreasing differences (even reversed in some cases for a system with 4:4 as the largest cluster size) in J with increasing maximal cluster implies that MA would show a significantly higher enhancing effect than DMA on MSA-driven NPF when larger cluster sizes are studied, consistent with previous experimental findings.[43] Therefore, combining all the above-mentioned analysis, it can be concluded that the basicity of amines is the determining factor that affects the formation of small $(DMA/MA)_{1-2}(MSA)_{1-2}$ clusters; however, the structural factors become more important in their further growth.

Formation Pathways. Figure 6 shows the cluster formation pathways for the DMA−MSA system obtained under conditions with 278.15 K, [MSA] = 10^6 cm^{-3}, and [base] = 10 ppt. The cluster formation pathways are also shown for the MA−MSA system as a comparison. As shown in Figure 6A, the formation of the $(DMA)_1(MSA)_1$ cluster is the first step of the cluster growth for the DMA−MSA system with the $(MSA)_2$ cluster only having a minor contribution. This mechanism is similar to that of the initial cluster growth in the MEA−MSA system.[29] Both the $(DMA)_1(MSA)_1$ and $(MSA)_2$ clusters grow to form $(DMA)_1(MSA)_2$ by colliding with MSA and DMA, respectively. After the formation of the $(DMA)_1(MSA)_2$ cluster, the cluster growth mainly proceeds via alternately adding one DMA monomer and one MSA monomer until the formation of the $(DMA)_3(MSA)_3$ cluster. The $(DMA)_3(MSA)_3$ cluster directly grows to form the $(DMA)_5(MSA)_5$ cluster via collision with $(DMA)_2(MSA)_2$.

https://dx.doi.org/10.1021/acs.est.0c05358
Environ. Sci. Technol. 2020, 54, 13498−13508

Such a unique growth pathway directly from $(DMA)_3(MSA)_3$ to the $(DMA)_5(MSA)_5$ cluster mainly results from the high stability of $(DMA)_2(MSA)_2$ and instability of $(DMA)_4(MSA)_4$, as shown by their ΔG values (Figure 2) or equivalent evaporation rates (Figure S5). For the formation of the $(DMA)_3(MSA)_3$ cluster, the collision of $(DMA)_2(MSA)_2$ with $(DMA)_1(MSA)_1$ has 22% contribution, with the dominant contribution being from the collision of $(DMA)_2(MSA)_3$ with a DMA molecule.

Overall, the growth pathway of the DMA−MSA system is different from that of the MA−MSA system. Three significant differences that deserve mentioning are as follows: (1) The initially formed cluster for the MA−MSA system is $(MSA)_2$ and not the $(base)_1(MSA)_1$ as for the DMA−MSA system. (2) The $(base)_1(MSA)_2$ cluster in the MA−MSA system has two equivalently important growth pathways: either adding one MA monomer or one MSA monomer to further form the larger $(base)_2(MSA)_3$ cluster. (3) The main growth pathway of the $(base)_3(MSA)_3$ cluster proceeds via a stepwise addition of MSA and base monomers for the MA−MSA system. This is a similar growth pathway as that in most other studied acid−base systems,[13,23,29] in contrast to the direct addition of a $(base)_2(MSA)_2$ cluster as found for the DMA−MSA system. The last difference implies that in the DMA−MSA system, the $(base)_3(MSA)_3$ cluster cannot efficiently grow to larger cluster sizes because the concentration of the $(base)_2(MSA)_2$ is much lower than that of MSA or the base monomer. Except for the difference, there is also one common feature for both systems in the growth pathway: the addition of MSA is more favorable than that of the base for the cluster with an equal number of acids and bases. This mainly come from the fact that $(base)_z(MSA)_{z+1}$ (z = 1−3) clusters are significantly more stable than the corresponding $(base)_{z+1}(MSA)_z$ (z = 1−3) clusters (based on the evaporation rates in the Supporting Information). This is consistent with the recent finding that small particles below 9 nm from MSA and MA are acidic.[74] In addition, the dominant growth pathways for both systems are kept when C_{coag} is changed (Supporting Information).

Atmospheric Implications. This study reveals that besides the H-bond capacity, the steric hindrance of the additional $-CH_3$ group in DMA is another structural factor that contributes to its lower enhancing potential on MSA-driven NPF, compared to MA. We noted that the number of the formed H-bonds for the protonated DMA with SA in the DMA−SA system is the same as that of the H-bonds for the protonated DMA with MSA in the corresponding DMA−MSA system (Table S2)[44] and no obvious additional steric repulsive energy was caused by the $-CH_3$ group of DMA in SA-driven NPF (Figure S11). In addition, both experimental and simulation studies confirm that DMA has much higher enhancing potential than MA on SA-driven NPF.[14,46] Therefore, although the lower H-bond capacity is an unfavorable factor in determining the enhancing potential of DMA on SA-driven NPF, it cannot counteract the increased enhancing potential caused by its higher gas-phase basicity compared to MA. One could argue that the lower H-bond capacity of DMA could be made up by the high H-bond capacity of SA. In fact, the number of H-bonds between SA and SA in the DMA−SA system is similar to that in the MA-SA system for $(base)_z(acid)_z$ (z = 2−4)[44] key clusters in their growth pathways. Therefore, in the view of H-bond formation, SA itself has little contribution to the difference in the enhancing potential between DMA and MA. Given the same number of the formed H-bonds for the protonated DMA in DMA−SA and DMA−MSA systems, the unfavorable contribution of the lower H-bond capacity on the enhancing potential in DMA−SA and DMA−MSA systems is roughly similar. Therefore, the additional steric hindrance caused by the additional $-CH_3$ group in DMA is responsible for reversing the trend in the enhancing potential of DMA and MA on MSA-driven NPF. This implies that the steric hindrance of the additional $-CH_3$ group of DMA plays an important role in determining its lower enhancing potential on MSA-driven NPF although it is difficult to directly estimate the contribution of the $-CH_3$ group. Together with the H-bond capacity and the basicity, the effect of potential steric hindrance should also be taken into account when screening species with high enhancing potential on MSA-driven NPF.

This study also reveals that the smallest DMA−MSA clusters are still more stable than the corresponding MA−MSA clusters within the 2:2 cluster size, indicating that the basicity of amines remains the dominant factor in the initial cluster formation. In the real ambient atmosphere, a broad variety of amines such as MA, DMA, TMA, and diamines likely coexist.[75] Therefore, MSA may initially bond with amines with strong basicity such as DMA or TMA to form stable small clusters, and then, amines with high enhancing potential when accounting for the steric hindrance, H-bond capacity, and basicity can further bond with the stable small clusters. In this way, atmospheric amines can synergistically enhance MSA-driven NPF and therefore further increase the role of atmospheric amines in MSA-driven NPF. It should be noted that a very recent experimental study has confirmed the synergetic effect of NH_3 in amine in enhancing MSA-driven NPF.[42] Given the significant role of amines in MSA-driven NPF, the synergetic effect of various amines, especially MA, DMA, and TMA, in enhancing MSA-driven NPF deserves further investigation. In addition, previous studies found the synergetic effect of MSA and SA in NPF in the presence of DMA and of atmospheric base in SA-driven NPF.[76] Because atmospheric bases, MSA, and SA can coexist over a broader range of current atmospheric conditions,[2] the NPF of mixed amines, ammonia, MSA, and SA could be important from the view of more realistic atmospheric conditions and is also warranted for future study.

■ ASSOCIATED CONTENT

Supporting Information

The Supporting Information is available free of charge at https://pubs.acs.org/doi/10.1021/acs.est.0c05358.

Details for the basic formula of the ACDC, judgement of cluster stability, selection of boundary clusters, effect of the coagulation sink coefficient on results, energy decomposition analysis based on the force field (EDA-FF), evaporation rates for DMA−MSA and MA−MSA clusters and various evaporation pathways of different clusters, number of H-bonds formed in clusters, thermodynamics information for the cluster formation, steady-state MSA dimer concentrations and cluster formation rates as a function of temperature, variation in the intermolecular S−S, O−O, N−N, and cluster density with cluster size, conformations of MA−MSA clusters, steady-state MSA dimer concentration and cluster formation rate with a "2 × 2 box" and "3 × 3 box" simulation for DMA−MSA and MA−MSA systems,

https://dx.doi.org/10.1021/acs.est.0c05358
Environ. Sci. Technol. 2020, 54, 13498−13508

repulsive energy for DMA/MA-SA clusters, and coordinates of all optimized DMA−MSA and MA−MSA clusters (PDF)

AUTHOR INFORMATION

Corresponding Author

Hong-Bin Xie − *Key Laboratory of Industrial Ecology and Environmental Engineering (Ministry of Education), School of Environmental Science and Technology, Dalian University of Technology, Dalian 116024, China;* orcid.org/0000-0002-9119-9785; Phone: +86-411-84707251; Email: hbxie@dlut.edu.cn

Authors

Jiewen Shen − *Key Laboratory of Industrial Ecology and Environmental Engineering (Ministry of Education), School of Environmental Science and Technology, Dalian University of Technology, Dalian 116024, China*

Jonas Elm − *Department of Chemistry and iClimate, Aarhus University, Aarhus C DK-8000, Denmark;* orcid.org/0000-0003-3736-4329

Jingwen Chen − *Key Laboratory of Industrial Ecology and Environmental Engineering (Ministry of Education), School of Environmental Science and Technology, Dalian University of Technology, Dalian 116024, China;* orcid.org/0000-0002-5756-3336

Junfeng Niu − *Research Center for Eco-environmental Engineering, Dongguan University of Technology, Dongguan 523808, China;* orcid.org/0000-0003-2592-3103

Hanna Vehkamäki − *Institute for Atmospheric and Earth System Research/Physics, University of Helsinki, Helsinki FI-00014, Finland;* orcid.org/0000-0002-5018-1255

Complete contact information is available at: https://pubs.acs.org/10.1021/acs.est.0c05358

Notes

The authors declare no competing financial interest.

ACKNOWLEDGMENTS

We thank Theo Kurtén from the University of Helsinki for expert advice. We thank the National Natural Science Foundation of China (21876024, 21677028), the Major International (Regional) Joint Research Project (21661142001), the Program for Changjiang Scholars and Innovative Research Team in University (IRT_13R05), the Programme of Introducing Talents of Discipline to Universities (B13012), Supercomputing Center of Dalian University of Technology, the European Research Council project 692891-Damocles, Academy of Finland, University of Helsinki, and Faculty of Science ATMATH project for funding.

REFERENCES

(1) Wang, M.; Kong, W.; Marten, R.; He, X.-C.; Chen, D.; Pfeifer, J.; Heitto, A.; Kontkanen, J.; Dada, L.; Kürten, A.; Yli-Juuti, T.; Manninen, H. E.; Amanatidis, S.; Amorim, A.; Baalbaki, R.; Baccarini, A.; Bell, D. M.; Bertozzi, B.; Bräkling, S.; Brilke, S.; Murillo, L. C.; Chiu, R.; Chu, B.; De Menezes, L.-P.; Duplissy, J.; Finkenzeller, H.; Carracedo, L. G.; Granzin, M.; Guida, R.; Hansel, A.; Hofbauer, V.; Krechmer, J.; Lehtipalo, K.; Lamkaddam, H.; Lampimäki, M.; Lee, C. P.; Makhmutov, V.; Marie, G.; Mathot, S.; Mauldin, R. L.; Mentler, B.; Müller, T.; Onnela, A.; Partoll, E.; Petäjä, T.; Philippov, M.; Pospisilova, V.; Ranjithkumar, A.; Rissanen, M.; Rörup, B.; Scholz, W.; Shen, J.; Simon, M.; Sipilä, M.; Steiner, G.; Stolzenburg, D.; Tham, Y. J.; Tomé, A.; Wagner, A. C.; Wang, D. S.; Wang, Y.; Weber, S. K.; Winkler, P. M.; Wlasits, P. J.; Wu, Y.; Xiao, M.; Ye, Q.; Zauner-Wieczorek, M.; Zhou, X.; Volkamer, R.; Riipinen, I.; Dommen, J.; Curtius, J.; Baltensperger, U.; Kulmala, M.; Worsnop, D. R.; Kirkby, J.; Seinfeld, J. H.; El-Haddad, I.; Flagan, R. C.; Donahue, N. M. Rapid Growth of New Atmospheric Particles by Nitric Acid and Ammonia Condensation. *Nature* **2020**, *581*, 184−189.

(2) Lee, S.-H.; Gordon, H.; Yu, H.; Lehtipalo, K.; Haley, R.; Li, Y.; Zhang, R. New Particle Formation in the Atmosphere: From Molecular Clusters to Global Climate. *J. Geophys. Res.: Atmos.* **2019**, *124*, 7098−7146.

(3) Yao, L.; Garmash, O.; Bianchi, F.; Zheng, J.; Yan, C.; Kontkanen, J.; Junninen, H.; Mazon, S. B.; Ehn, M.; Paasonen, P.; Sipilä, M.; Wang, M.; Wang, X.; Xiao, S.; Chen, H.; Lu, Y.; Zhang, B.; Wang, D.; Fu, Q.; Geng, F.; Li, L.; Wang, H.; Qiao, L.; Yang, X.; Chen, J.; Kerminen, V.-M.; Petäjä, T.; Worsnop, D. R.; Kulmala, M.; Wang, L. Atmospheric New Particle Formation from Sulfuric Acid and Amines in A Chinese Megacity. *Science* **2018**, *361*, 278.

(4) Riccobono, F.; Schobesberger, S.; Scott, C. E.; Dommen, J.; Ortega, I. K.; Rondo, L.; Almeida, J.; Amorim, A.; Bianchi, F.; Breitenlechner, M.; David, A.; Downard, A.; Dunne, E. M.; Duplissy, J.; Ehrhart, S.; Flagan, R. C.; Franchin, A.; Hansel, A.; Junninen, H.; Kajos, M.; Keskinen, H.; Kupc, A.; Kurten, A.; Kvashin, A. N.; Laaksonen, A.; Lehtipalo, K.; Makhmutov, V.; Mathot, S.; Nieminen, T.; Onnela, A.; Petaja, T.; Praplan, A. P.; Santos, F. D.; Schallhart, S.; Seinfeld, J. H.; Sipila, M.; Spracklen, D. V.; Stozhkov, Y.; Stratmann, F.; Tome, A.; Tsagkogeorgas, G.; Vaattovaara, P.; Viisanen, Y.; Vrtala, A.; Wagner, P. E.; Weingartner, E.; Wex, H.; Wimmer, D.; Carslaw, K. S.; Curtius, J.; Donahue, N. M.; Kirkby, J.; Kulmala, M.; Worsnop, D. R.; Baltensperger, U. Oxidation Products of Biogenic Emissions Contribute to Nucleation of Atmospheric Particles. *Science* **2014**, *344*, 717−721.

(5) Zhang, R.; Khalizov, A.; Wang, L.; Hu, M.; Xu, W. Nucleation and Growth of Nanoparticles in the Atmosphere. *Chem. Rev.* **2012**, *112*, 1957−2011.

(6) Kirkby, J.; Curtius, J.; Almeida, J.; Dunne, E.; Duplissy, J.; Ehrhart, S.; Franchin, A.; Gagné, S.; Ickes, L.; Kürten, A.; Kupc, A.; Metzger, A.; Riccobono, F.; Rondo, L.; Schobesberger, S.; Tsagkogeorgas, G.; Wimmer, D.; Amorim, A.; Bianchi, F.; Breitenlechner, M.; David, A.; Dommen, J.; Downard, A.; Ehn, M.; Flagan, R. C.; Haider, S.; Hansel, A.; Hauser, D.; Jud, W.; Junninen, H.; Kreissl, F.; Kvashin, A.; Laaksonen, A.; Lehtipalo, K.; Lima, J.; Lovejoy, E. R.; Makhmutov, V.; Mathot, S.; Mikkilä, J.; Minginette, P.; Mogo, S.; Nieminen, T.; Onnela, A.; Pereira, P.; Petäjä, T.; Schnitzhofer, R.; Seinfeld, J. H.; Sipilä, M.; Stozhkov, Y.; Stratmann, F.; Tomé, A.; Vanhanen, J.; Viisanen, Y.; Vrtala, A.; Wagner, P. E.; Walther, H.; Weingartner, E.; Wex, H.; Winkler, P. M.; Carslaw, K. S.; Worsnop, D. R.; Baltensperger, U.; Kulmala, M. Role of Sulphuric Acid, Ammonia and Galactic Cosmic Rays in Atmospheric Aerosol Nucleation. *Nature* **2011**, *476*, 429−433.

(7) Liu, L.; Zhong, J.; Vehkamäki, H.; Kurtén, T.; Du, L.; Zhang, X.; Francisco, J. S.; Zeng, X. C. Unexpected quenching effect on new particle formation from the atmospheric reaction of methanol with SO_3. *Proc. Natl. Acad. Sci. U.S.A.* **2019**, *116*, 24966−24971.

(8) Feketeová, L.; Bertier, P.; Salbaing, T.; Azuma, T.; Calvo, F.; Farizon, B.; Farizon, M.; Märk, T. D. Impact of A Hydrophobic Ion on the Early Stage of Atmospheric Aerosol Formation. *Proc. Natl. Acad. Sci. U.S.A.* **2019**, *116*, 22540−22544.

(9) Rose, C.; Zha, Q.; Dada, L.; Yan, C.; Lehtipalo, K.; Junninen, H.; Mazon, S. B.; Jokinen, T.; Sarnela, N.; Sipilä, M.; Petäjä, T.; Kerminen, V.-M.; Bianchi, F.; Kulmala, M. Observations of Biogenic Ion-induced Cluster Formation in the Atmosphere. *Sci. Adv.* **2018**, *4*, No. eaar5218.

(10) Chen, H.; Finlayson-Pitts, B. J. New Particle Formation from Methanesulfonic Acid and Amines/Ammonia as a Function of Temperature. *Environ. Sci. Technol.* **2017**, *51*, 243−252.

(11) Kirkby, J.; Duplissy, J.; Sengupta, K.; Frege, C.; Gordon, H.; Williamson, C.; Heinritzi, M.; Simon, M.; Yan, C.; Almeida, J.; Tröstl, J.; Nieminen, T.; Ortega, I. K.; Wagner, R.; Adamov, A.; Amorim, A.; Bernhammer, A.-K.; Bianchi, F.; Breitenlechner, M.; Brilke, S.; Chen, X.; Craven, J.; Dias, A.; Ehrhart, S.; Flagan, R. C.; Franchin, A.; Fuchs, C.; Guida, R.; Hakala, J.; Hoyle, C. R.; Jokinen, T.; Junninen, H.; Kangasluoma, J.; Kim, J.; Krapf, M.; Kürten, A.; Laaksonen, A.; Lehtipalo, K.; Makhmutov, V.; Mathot, S.; Molteni, U.; Onnela, A.; Peräkylä, O.; Piel, F.; Petäjä, T.; Praplan, A. P.; Pringle, K.; Rap, A.; Richards, N. A. D.; Riipinen, I.; Rissanen, M. P.; Rondo, L.; Sarnela, N.; Schobesberger, S.; Scott, C. E.; Seinfeld, J. H.; Sipilä, M.; Steiner, G.; Stozhkov, Y.; Stratmann, F.; Tomé, A.; Virtanen, A.; Vogel, A. L.; Wagner, A. C.; Wagner, P. E.; Weingartner, E.; Wimmer, D.; Winkler, P. M.; Ye, P.; Zhang, X.; Hansel, A.; Dommen, J.; Donahue, N. M.; Worsnop, D. R.; Baltensperger, U.; Kulmala, M.; Carslaw, K. S.; Curtius, J. Ion-induced Nucleation of Pure Biogenic Particles. *Nature* **2016**, *533*, 521−526.

(12) Schobesberger, S.; Junninen, H.; Bianchi, F.; Lonn, G.; Ehn, M.; Lehtipalo, K.; Dommen, J.; Ehrhart, S.; Ortega, I. K.; Franchin, A.; Nieminen, T.; Riccobono, F.; Hutterli, M.; Duplissy, J.; Almeida, J.; Amorim, A.; Breitenlechner, M.; Downard, A. J.; Dunne, E. M.; Flagan, R. C.; Kajos, M.; Keskinen, H.; Kirkby, J.; Kupc, A.; Kurten, A.; Kurten, T.; Laaksonen, A.; Mathot, S.; Onnela, A.; Praplan, A. P.; Rondo, L.; Santos, F. D.; Schallhart, S.; Schnitzhofer, R.; Sipila, M.; Tome, A.; Tsagkogeorgas, G.; Vehkamaki, H.; Wimmer, D.; Baltensperger, U.; Carslaw, K. S.; Curtius, J.; Hansel, A.; Petaja, T.; Kulmala, M.; Donahue, N. M.; Worsnop, D. R. Molecular Understanding of Atmospheric Particle Formation from Sulfuric Acid and Large Oxidized Organic Molecules. *Proc. Natl. Acad. Sci. U.S.A.* **2013**, *110*, 17223−17228.

(13) Xie, H.-B.; Elm, J.; Halonen, R.; Myllys, N.; Kurtén, T.; Kulmala, M.; Vehkamäki, H. Atmospheric Fate of Monoethanolamine: Enhancing New Particle Formation of Sulfuric Acid as an Important Removal Process. *Environ. Sci. Technol.* **2017**, *51*, 8422−8431.

(14) Olenius, T.; Halonen, R.; Kurtén, T.; Henschel, H.; Kupiainen-Määttä, O.; Ortega, I. K.; Jen, C. N.; Vehkamäki, H.; Riipinen, I. New particle formation from sulfuric acid and amines: Comparison of monomethylamine, dimethylamine, and trimethylamine. *J. Geophys. Res.: Atmos.* **2017**, *122*, 7103−7118.

(15) Lehtipalo, K.; Rondo, L.; Kontkanen, J.; Schobesberger, S.; Jokinen, T.; Sarnela, N.; Kuerten, A.; Ehrhart, S.; Franchin, A.; Nieminen, T.; Riccobono, F.; Sipila, M.; Yli-Juuti, T.; Duplissy, J.; Adamov, A.; Ahlm, L.; Almeida, J.; Amorim, A.; Bianchi, F.; Breitenlechner, M.; Dommen, J.; Downard, A. J.; Dunne, E. M.; Flagan, R. C.; Guida, R.; Hakala, J.; Hansel, A.; Jud, W.; Kangasluoma, J.; Kerminen, V.-M.; Keskinen, H.; Kim, J.; Kirkby, J.; Kupc, A.; Kupiainen-Maatta, O.; Laaksonen, A.; Lawler, M. J.; Leiminger, M.; Mathot, S.; Olenius, T.; Ortega, I. K.; Onnela, A.; Petaja, T.; Praplan, A.; Rissanen, M. P.; Ruuskanen, T.; Santos, F. D.; Schallhart, S.; Schnitzhofer, R.; Simon, M.; Smith, J. N.; Trostl, J.; Tsagkogeorgas, G.; Tome, A.; Vaattovaara, P.; Vehkamaki, H.; Vrtala, A. E.; Wagner, P. E.; Williamson, C.; Wimmer, D.; Winkler, P. M.; Virtanen, A.; Donahue, N. M.; Carslaw, K. S.; Baltensperger, U.; Riipinen, I.; Curtius, J.; Worsnop, D. R.; Kulmala, M. The Effect of Acid-base Clustering and Ions on the Growth of Atmospheric Nano-particles. *Nat. Commun.* **2016**, *7*, 11594.

(16) Chen, M.; Titcombe, M.; Jiang, J.; Jen, C.; Kuang, C.; Fischer, M. L.; Eisele, F. L.; Siepmann, J. I.; Hanson, D. R.; Zhao, J.; McMurry, P. H. Acid-base Chemical Reaction Model for Nucleation Rates in the Polluted Atmospheric Boundary Layer. *Proc. Natl. Acad. Sci. U.S.A.* **2012**, *109*, 18713−18718.

(17) Zhao, J.; Smith, J. N.; Eisele, F. L.; Chen, M.; Kuang, C.; McMurry, P. H. Observation of Neutral Sulfuric Acid-amine Containing Clusters in Laboratory and Ambient Measurements. *Atmos. Chem. Phys.* **2011**, *11*, 10823−10836.

(18) Erupe, M. E.; Viggiano, A. A.; Lee, S.-H. The Effect of Trimethylamine on Atmospheric Nucleation Involving H_2SO_4. *Atmos. Chem. Phys.* **2011**, *11*, 4767−4775.

(19) Sipilä, M.; Berndt, T.; Petäjä, T.; Brus, D.; Vanhanen, J.; Stratmann, F.; Patokoski, J.; Mauldin, R. L.; Hyvärinen, A.-P.; Lihavainen, H.; Kulmala, M. The Role of Sulfuric Acid in Atmospheric Nucleation. *Science* **2010**, *327*, 1243−1246.

(20) Loukonen, V.; Kurtén, T.; Ortega, I. K.; Vehkamäki, H.; Pádua, A. A. H.; Sellegri, K.; Kulmala, M. Enhancing effect of dimethylamine in sulfuric acid nucleation in the presence of water - a computational study. *Atmos. Chem. Phys.* **2010**, *10*, 4961−4974.

(21) Kurtén, T.; Kuang, C.; Gómez, P.; McMurry, P. H.; Vehkamäki, H.; Ortega, I.; Noppel, M.; Kulmala, M. The Role of Cluster Energy Nonaccommodation in Atmospheric Sulfuric Acid Nucleation. *J. Chem. Phys.* **2010**, *132*, 024304.

(22) Murphy, S. M.; Sorooshian, A.; Kroll, J. H.; Ng, N. L.; Chhabra, P.; Tong, C.; Surratt, J. D.; Knipping, E.; Flagan, R. C.; Seinfeld, J. H. Secondary Aerosol Formation from Atmospheric Reactions of Aliphatic Amines. *Atmos. Chem. Phys.* **2007**, *7*, 2313−2337.

(23) Ma, F.; Xie, H.-B.; Elm, J.; Shen, J.; Chen, J.; Vehkamäki, H. Piperazine Enhancing Sulfuric Acid-Based New Particle Formation: Implications for the Atmospheric Fate of Piperazine. *Environ. Sci. Technol.* **2019**, *53*, 8785−8795.

(24) Jen, C. N.; McMurry, P. H.; Hanson, D. R. Stabilization of Sulfuric Acid Dimers by Ammonia, Methylamine, Dimethylamine, and Trimethylamine. *J. Geophys. Res.: Atmos.* **2014**, *119*, 7502−7514.

(25) Almeida, J.; Schobesberger, S.; Kürten, A.; Ortega, I. K.; Kupiainen-Määttä, O.; Praplan, A. P.; Adamov, A.; Amorim, A.; Bianchi, F.; Breitenlechner, M.; David, A.; Dommen, J.; Donahue, N. M.; Downard, A.; Dunne, E.; Duplissy, J.; Ehrhart, S.; Flagan, R. C.; Franchin, A.; Guida, R.; Hakala, J.; Hansel, A.; Heinritzi, M.; Henschel, H.; Jokinen, T.; Junninen, H.; Kajos, M.; Kangasluoma, J.; Keskinen, H.; Kupc, A.; Kurtén, T.; Kvashin, A. N.; Laaksonen, A.; Lehtipalo, K.; Leiminger, M.; Leppä, J.; Loukonen, V.; Makhmutov, V.; Mathot, S.; McGrath, M. J.; Nieminen, T.; Olenius, T.; Onnela, A.; Petäjä, T.; Riccobono, F.; Riipinen, I.; Rissanen, M.; Rondo, L.; Ruuskanen, T.; Santos, F. D.; Sarnela, N.; Schallhart, S.; Schnitzhofer, R.; Seinfeld, J. H.; Simon, M.; Sipilä, M.; Stozhkov, Y.; Stratmann, F.; Tomé, A.; Tröstl, J.; Tsagkogeorgas, G.; Vaattovaara, P.; Viisanen, Y.; Virtanen, A.; Vrtala, A.; Wagner, P. E.; Weingartner, E.; Wex, H.; Williamson, C.; Wimmer, D.; Ye, P.; Yli-Juuti, T.; Carslaw, K. S.; Kulmala, M.; Curtius, J.; Baltensperger, U.; Worsnop, D. R.; Vehkamäki, H.; Kirkby, J. Molecular Understanding of Sulphuric Acid-amine Particle Nucleation in the Atmosphere. *Nature* **2013**, *502*, 359−363.

(26) Zhang, R.; Wang, L.; Khalizov, A. F.; Zhao, J.; Zheng, J.; McGraw, R. L.; Molina, L. T. Formation of Nanoparticles of Blue Haze Enhanced by Anthropogenic Pollution. *Proc. Natl. Acad. Sci. U.S.A.* **2009**, *106*, 17650−17654.

(27) Kurtén, T.; Loukonen, V.; Vehkamäki, H.; Kulmala, M. Amines Are Likely to Enhance Neutral and Ion-induced Sulfuric Acid-water Nucleation in the Atmosphere More Effectively than Ammonia. *Atmos. Chem. Phys.* **2008**, *8*, 4095−4103.

(28) Zhang, R.; Suh, I.; Zhao, J.; Zhang, D.; Fortner, E. C.; Tie, X. X.; Molina, L. T.; Molina, M. J. Atmospheric New Particle Formation Enhanced by Organic Acids. *Science* **2004**, *304*, 1487−1490.

(29) Shen, J.; Xie, H.-B.; Elm, J.; Ma, F.; Chen, J.; Vehkamäki, H. Methanesulfonic Acid-driven New Particle Formation Enhanced by Monoethanolamine: A Computational Study. *Environ. Sci. Technol.* **2019**, *53*, 14387−14397.

(30) Ehn, M.; Thornton, J. A.; Kleist, E.; Sipilä, M.; Junninen, H.; Pullinen, I.; Springer, M.; Rubach, F.; Tillmann, R.; Lee, B.; Lopez-Hilfiker, F.; Andres, S.; Acir, I.-H.; Rissanen, M.; Jokinen, T.; Schobesberger, S.; Kangasluoma, J.; Kontkanen, J.; Nieminen, T.; Kurtén, T.; Nielsen, L. B.; Jørgensen, S.; Kjaergaard, H. G.; Canagaratna, M.; Maso, M. D.; Berndt, T.; Petäjä, T.; Wahner, A.; Kerminen, V.-M.; Kulmala, M.; Worsnop, D. R.; Mentel, T. F.; Mentel, T. F. A Large Source of Low-volatility Secondary Organic Aerosol. *Nature* **2014**, *506*, 476−479.

(31) Dawson, M. L.; Varner, M. E.; Perraud, V.; Ezell, M. J.; Gerber, R. B.; Finlayson-Pitts, B. J. Simplified Mechanism for New Particle Formation from Methanesulfonic Acid, Amines, and Water via

https://dx.doi.org/10.1021/acs.est.0c05358
Environ. Sci. Technol. 2020, 54, 13498−13508

Experiments and ab initio Calculations. *Proc. Natl. Acad. Sci. U.S.A.* **2012**, *109*, 18719−18724.
(32) Wehner, B.; Petäjä, T.; Boy, M.; Engler, C.; Birmili, W.; Tuch, T.; Wiedensohler, A.; Kulmala, M. The Contribution of Sulfuric Acid and Non-volatile Compounds on the Growth of Freshly Formed Atmospheric Aerosols. *Geophys. Res. Lett.* **2005**, *32*, L17810.
(33) Hodshire, A. L.; Campuzano-Jost, P.; Kodros, J. K.; Croft, B.; Nault, B. A.; Schroder, J. C.; Jimenez, J. L.; Pierce, J. R. The Potential Role of Methanesulfonic Acid (MSA) in Aerosol Formation and Growth and the Associated Radiative Forcings. *Atmos. Chem. Phys.* **2019**, *19*, 3137−3160.
(34) Arquero, K. D.; Xu, J.; Gerber, R. B.; Finlayson-Pitts, B. J. Particle Formation and Growth from Oxalic Acid, Methanesulfonic Acid, Trimethylamine and Water: a Combined Experimental and Theoretical Study. *Phys. Chem. Chem. Phys.* **2017**, *19*, 28286−28301.
(35) Perraud, V.; Horne, J. R.; Martinez, A. S.; Kalinowski, J.; Meinardi, S.; Dawson, M. L.; Wingen, L. M.; Dabdub, D.; Blake, D. R.; Gerber, R. B.; Finlayson-Pitts, B. J. The Future of Airborne Sulfur-containing Particles in the Absence of Fossil Fuel Sulfur Dioxide Emissions. *Proc. Natl. Acad. Sci. U.S.A.* **2015**, *112*, 13514−13519.
(36) Hopkins, R. J.; Desyaterik, Y.; Tivanski, A. V.; Zaveri, R. A.; Berkowitz, C. M.; Tyliszczak, T.; Gilles, M. K.; Laskin, A. Chemical Speciation of Sulfur in Marine Cloud Droplets and Particles: Analysis of Individual Particles from the Marine Boundary Layer over the California Current. *J. Geophys. Res.: Atmos.* **2008**, *113*, 209.
(37) Stern, D. I. Global Sulfur Emissions from 1850 to 2000. *Chemosphere* **2005**, *58*, 163−175.
(38) Veres, P. R.; Neuman, J. A.; Bertram, T. H.; Assaf, E.; Wolfe, G. M.; Williamson, C. J.; Weinzierl, B.; Tilmes, S.; Thompson, C. R.; Thames, A. B.; Schroder, J. C.; Saiz-Lopez, A.; Rollins, A. W.; Roberts, J. M.; Price, D.; Peischl, J.; Nault, B. A.; Møller, K. H.; Miller, D. O.; Meinardi, S.; Li, Q.; Lamarque, J.-F.; Kupc, A.; Kjaergaard, H. G.; Kinnison, D.; Jimenez, J. L.; Jernigan, C. M.; Hornbrook, R. S.; Hills, A.; Dollner, M.; Day, D. A.; Cuevas, C. A.; Campuzano-Jost, P.; Burkholder, J.; Bui, T. P.; Brune, W. H.; Brown, S. S.; Brock, C. A.; Bourgeois, I.; Blake, D. R.; Apel, E. C.; Ryerson, T. B. Global Airborne Sampling Reveals A Previously Unobserved Dimethyl Sulfide Oxidation Mechanism in the Marine Atmosphere. *Proc. Natl. Acad. Sci. U.S.A.* **2020**, *117*, 4505−4510.
(39) Ning, A.; Zhang, H.; Zhang, X.; Li, Z.; Zhang, Y.; Xu, Y.; Ge, M. A Molecular-scale Study on the Role of Methanesulfinic Acid in Marine New Particle Formation. *Atmos. Environ.* **2020**, *227*, 117378.
(40) Barnes, I.; Hjorth, J.; Mihalopoulos, N. Dimethyl Sulfide and Dimethyl Sulfoxide and Their Oxidation in the Atmosphere. *Chem. Rev.* **2006**, *106*, 940−975.
(41) Eisele, F. L.; Tanner, D. J. Measurement of the gas phase concentration of H_2SO_4 and methane sulfonic acid and estimates of H_2SO_4 production and loss in the atmosphere. *J. Geophys. Res.: Atmos.* **1993**, *98*, 9001−9010.
(42) Perraud, V.; Xu, J.; Gerber, R. B.; Finlayson-Pitts, B. J. Integrated Experimental and Theoretical Approach to Probe the Synergistic Effect of Ammonia in Methanesulfonic Acid Reactions with Small Alkylamines. *Environ. Sci.: Processes Impacts* **2020**, *22*, 305−328.
(43) Chen, H.; Varner, M. E.; Gerber, R. B.; Finlayson-Pitts, B. J. Reactions of Methanesulfonic Acid with Amines and Ammonia as a Source of New Particles in Air. *J. Phys. Chem. B* **2016**, *120*, 1526−1536.
(44) Elm, J. An Atmospheric Cluster Database Consisting of Sulfuric Acid, Bases, Organics, and Water. *ACS Omega* **2019**, *4*, 10965−10974.
(45) Waller, S. E.; Yang, Y.; Castracane, E.; Racow, E. E.; Kreinbihl, J. J.; Nickson, K. A.; Johnson, C. J. The Interplay Between Hydrogen Bonding and Coulombic Forces in Determining the Structure of Sulfuric Acid-Amine Clusters. *J. Phys. Chem. Lett.* **2018**, *9*, 1216−1222.
(46) Glasoe, W. A.; Volz, K.; Panta, B.; Freshour, N.; Bachman, R.; Hanson, D. R.; McMurry, P. H.; Jen, C. Sulfuric Acid Nucleation: An Experimental Study of the Effect of Seven Bases. *J. Geophys. Res.: Atmos.* **2015**, *120*, 1933−1950.
(47) Elm, J.; Jen, C. N.; Kurtén, T.; Vehkamäki, H. Strong Hydrogen Bonded Molecular Interactions between Atmospheric Diamines and Sulfuric Acid. *J. Phys. Chem. A* **2016**, *120*, 3693−3700.
(48) Xu, J.; Perraud, V.; Finlayson-Pitts, B. J.; Gerber, R. B. Uptake of Water by an Acid-base Nanoparticle: Theoretical and Experimental Studies of the Methanesulfonic Acid-methylamine System. *Phys. Chem. Chem. Phys.* **2018**, *20*, 22249−22259.
(49) Arquero, K. D.; Gerber, R. B.; Finlayson-Pitts, B. J. The Role of Oxalic Acid in New Particle Formation from Methanesulfonic Acid, Methylamine, and Water. *Environ. Sci. Technol.* **2017**, *51*, 2124−2130.
(50) Chen, H.; Ezell, M. J.; Arquero, K. D.; Varner, M. E.; Dawson, M. L.; Gerber, R. B.; Finlayson-Pitts, B. J. New Particle Formation and Growth from Methanesulfonic Acid, Trimethylamine and Water. *Phys. Chem. Chem. Phys.* **2015**, *17*, 13699−13709.
(51) Dawson, M. L.; Varner, M. E.; Perraud, V.; Ezell, M. J.; Wilson, J.; Zelenyuk, A.; Gerber, R. B.; Finlayson-Pitts, B. J. Amine-Amine Exchange in Aminium-Methanesulfonate Aerosols. *J. Phys. Chem. C* **2014**, *118*, 29431−29440.
(52) Nishino, N.; Arquero, K. D.; Dawson, M. L.; Finlayson-Pitts, B. J. Infrared Studies of the Reaction of Methanesulfonic Acid with Trimethylamine on Surfaces. *Environ. Sci. Technol.* **2014**, *48*, 323−330.
(53) Xu, J.; Finlayson-Pitts, B. J.; Gerber, R. B. Nanoparticles Grown from Methanesulfonic Acid and Methylamine: Microscopic Structures and Formation Mechanism. *Phys. Chem. Chem. Phys.* **2017**, *19*, 31949−31957.
(54) Xu, J.; Finlayson-Pitts, B. J.; Gerber, R. B. Proton Transfer in Mixed Clusters of Methanesulfonic Acid, Methylamine, and Oxalic Acid: Implications for Atmospheric Particle Formation. *J. Phys. Chem. A* **2017**, *121*, 2377−2385.
(55) Hunter, E. P. L.; Lias, S. G. Evaluated Gas Phase Basicities and Proton Affinities of Molecules: An Update. *J. Phys. Chem. Ref. Data* **1998**, *27*, 413−656.
(56) Kumar, M.; Shee, J.; Rudshteyn, B.; Reichman, D. R.; Friesner, R. A.; Miller, C. E.; Francisco, J. S. Multiple Stable Isoprene-Ozone Complexes Reveal Complex Entrance Channel Dynamics in the Isoprene + Ozone Reaction. *J. Am. Chem. Soc.* **2020**, *142*, 10806−10813.
(57) Tian, A.-x.; Yang, Y.; Ying, J.; Li, N.; Lin, X.-l.; Zhang, J.-w.; Wang, X.-l. The key role of -CH_3 steric hindrance in bis(pyrazolyl) ligand on polyoxometalate-based compounds. *Dalton Trans.* **2014**, *43*, 8405−8413.
(58) Chen, D.; Li, D.; Wang, C.; Luo, Y.; Liu, F.; Wang, W. Atmospheric Implications of Hydration on the Formation of Methanesulfonic Acid and Methylamine Clusters: A Theoretical Study. *Chemosphere* **2020**, *244*, 125538.
(59) McGrath, M. J.; Olenius, T.; Ortega, I. K.; Loukonen, V.; Paasonen, P.; Kurtén, T.; Kulmala, M.; Vehkamäki, H. Atmospheric Cluster Dynamics Code: a flexible method for solution of the birth-death equations. *Atmos. Chem. Phys.* **2012**, *12*, 2345−2355.
(60) Frisch, M. J.; Trucks, G. W.; Schlegel, H. B.; Scuseria, G. E.; Robb, M. A.; Cheeseman, J. R.; Scalmani, G.; Barone, V.; Mennucci, B.; Petersson, G. A.; Nakatsuji, H.; Caricato, M.; Li, X.; Hratchian, H. P.; Izmaylov, A. F.; Bloino, J.; Zheng, G.; Sonnenberg, J. L.; Hada, M.; Ehara, M.; Toyota, K.; Fukuda, R.; Hasegawa, J.; Ishida, M.; Nakajima, T.; Honda, Y.; Kitao, O.; Nakai, H.; Vreven, T.; Montgomery, J. A., Jr; Peralta, J. E.; Ogliaro, F.; Bearpark, M.; Heyd, J. J.; Brothers, E.; Kudin, K. N.; Staroverov, V. N.; Kobayashi, R.; Normand, J.; Raghavachari, K.; Rendell, A.; Burant, J. C.; Iyengar, S. S.; Tomasi, J.; Cossi, M.; Rega, N.; Millam, J. M.; Klene, M.; Knox, J. E.; Cross, J. B.; Bakken, V.; Adamo, C.; Jaramillo, J.; Gomperts, R.; Stratmann, R. E.; Yazyev, O.; Austin, A. J.; Cammi, R.; Pomelli, C.; Ochterski, J. W.; Martin, R. L.; Morokuma, K.; Zakrzewski, V. G.; Voth, G. A.; Salvador, P.; Dannenberg, J. J.; Dapprich, S.; Daniels, A. D.; Farkas, O.; Foresman, J. B.; Ortiz, J. V.; Cioslowski, J.; Fox, D. J. *Gaussian 09*; Gaussian Inc., 2009.

https://dx.doi.org/10.1021/acs.est.0c05358
Environ. Sci. Technol. 2020, 54, 13498−13508

(61) Neese, F. The ORCA program system. *Wiley Interdiscip. Rev.: Comput. Mol. Sci.* **2012**, *2*, 73−78.
(62) Elm, J.; Kubečka, J.; Besel, V.; Jääskeläinen, M. J.; Halonen, R.; Kurtén, T.; Vehkamäki, H. Modeling the formation and growth of atmospheric molecular clusters: A review. *J. Aerosol Sci.* **2020**, *149*, 105621.
(63) Jayaratne, R.; Pushpawela, B.; He, C.; Li, H.; Gao, J.; Chai, F.; Morawska, L. Observations of Particles at Their Formation Sizes in Beijing, China. *Atmos. Chem. Phys.* **2017**, *17*, 8825−8835.
(64) Qi, X. M.; Ding, A. J.; Nie, W.; Petäjä, T.; Kerminen, V.-M.; Herrmann, E.; Xie, Y. N.; Zheng, L. F.; Manninen, H.; Aalto, P.; Sun, J. N.; Xu, Z. N.; Chi, X. G.; Huang, X.; Boy, M.; Virkkula, A.; Yang, X.-Q.; Fu, C. B.; Kulmala, M. Aerosol Size Distribution and New Particle Formation in the Western Yangtze River Delta of China: 2 Years of Measurements at the SORPES Station. *Atmos. Chem. Phys.* **2015**, *15*, 12445−12464.
(65) Nicklaus, M. C.; Wang, S.; Driscoll, J. S.; Milne, G. W. A. Conformational changes of small molecules binding to proteins. *Bioorg. Med. Chem.* **1995**, *3*, 411−428.
(66) Almarsson, O.; Bruice, T. C. Evaluation of the factors influencing reactivity and stereospecificity in NAD(P)H dependent dehydrogenase enzymes. *J. Am. Chem. Soc.* **1993**, *115*, 2125−2138.
(67) Lu, T.; Chen, F. Multiwfn: A Multifunctional Wavefunction Analyzer. *J. Comput. Chem.* **2012**, *33*, 580−592.
(68) Chen, Z.; Han, R.; Zhong, C. Adsorption of Fluoroquinolone by Carbon Nanotubes: A Combined Experimental and Density Functional Theory Study. *Chem. Pap.* **2020**, *74*, 3847−3856.
(69) Zhu, S.-f.; Gan, Q.; Feng, C. Multimolecular Complexes of CL-20 with Nitropyrazole Derivatives: Geometric, Electronic Structure, and Stability. *ACS Omega* **2019**, *4*, 13408−13417.
(70) Zhan, K.; Li, Z.; Chen, J.; Hou, Y.; Zhang, J.; Sun, R.; Bu, Z.; Wang, L.; Wang, M.; Chen, X.; Hou, X. Tannic Acid Modified Single Nanopore with Multivalent Metal Ions Recognition and Ultra-trace Level Detection. *Nano Today* **2020**, *33*, 100868.
(71) Zheng, A.; Ren, M.; Zhang, Y.; Cai, Y.; Zhang, J.; Yuan, Y.; Lei, M.; Wang, P. A Thioxanthenothioxanthene-based Hole Transporter with 2D Molecular Stacking for Efficient and Thermostable Perovskite Solar Cells. *ACS Mater. Lett.* **2020**, *2*, 691−698.
(72) Chandra, A. Effects of Ion Atmosphere on Hydrogen-bond Dynamics in Aqueous Electrolyte Solutions. *Phys. Rev. Lett.* **2000**, *85*, 768−771.
(73) Lu, T.; Chen, F. Quantitative Analysis of Molecular Surface Based on Improved Marching Tetrahedra Algorithm. *J. Mol. Graph.* **2012**, *38*, 314−323.
(74) Perraud, V.; Li, X.; Jiang, J.; Finlayson-Pitts, B. J.; Smith, J. N. Size-Resolved Chemical Composition of Sub-20 nm Particles from Methanesulfonic Acid Reactions with Methylamine and Ammonia. *ACS Earth Space Chem.* **2020**, *4*, 1182−1194.
(75) Ge, X.; Wexler, A. S.; Clegg, S. L. Atmospheric Amines - Part I. A review. *Atmos. Environ.* **2011**, *45*, 524−546.
(76) Bork, N.; Elm, J.; Olenius, T.; Vehkamäki, H. Methane Sulfonic Acid-Enhanced Formation of Molecular Clusters of Sulfuric Acid and Dimethyl Amine. *Atmos. Chem. Phys.* **2014**, *14*, 12023−12030.

https://dx.doi.org/10.1021/acs.est.0c05358
Environ. Sci. Technol. 2020, 54, 13498−13508